NONLINEAR SURFACE ACOUSTIC WAVES IN MATERIALS SCIENCE

P. Hess, A. M. Lomonosov
Institute of Physical Chemistry, INF 253
University of Heidelberg
69120 Heidelberg, Germany
peter.hess@urz.uni-heidelberg.de

Abstract

Laser-generated nonlinear surface acoustic wave pulses provide a novel tool for studying the nonlinear mechanical behavior of isotropic and anisotropic materials, including the formation of solitary surface pulses, shock fronts, and mechanical failure. The bond disruption process, occurring when the stress exceeds the mechanical strength, limits the SAW amplitudes and acoustic Mach numbers that can be achieved in nonlinear surface waves.

Introduction

Nonlinear surface acoustic waves (SAWs) can be generated by strongly focusing pulsed laser radiation to a line onto a sample surface [1]. In this way a plane surface wave is launched, propagating in a well-defined direction. The particle motion is elliptically polarized with a longitudinal or in-plane component and a shear or out-of-plane displacement component. The transient shear distortions of the surface can be detected at two distances from the excitation source by laser probe beam deflection monitored with position-sensitive detectors [1]. The two-point probe technique is crucial for a comparison between experiment and theory. To be independent of the properties of the source the waveform measured at the first probe spot is used as input SAW profile for solving the evolution equation. The pulse shape calculated for the second probe spot is then compared with the experiment.

For finite SAW pulses, excited by the "absorption-layer method" [2], the shock formation distance may be smaller than the attenuation length. In this case frequency-up conversion ("formation of shocks") takes place during propagation and the elastic surface pulses develop spikes and shock fronts during nonlinear evolution. Since a surface wave penetrates only on the order of one wavelength deep into the solid, frequency-up conversion is connected with a concentration of elastic energy nearer to the surface. In reality, both shortening and lengthening of the elastic pulses may be observed during nonlinear evolution. In amorphous materials, such as fused quartz or silica, the nonlinear behavior is isotropic, whereas in anisotropic single crystals, such as silicon, these effects may vary strongly with the crystallographic plane and direction of nonlinear SAW propagation [3].

The amplitude of deformation and strain that can be achieved in such nonlinear SAW pulses is ultimately limited by the mechanical strength of the material. If we define the acoustic Mach number by the ratio of the surface velocity to the phase velocity or by the ratio of the surface displacement to the wavelength of the SAW pulse, Mach numbers in the range of 0.01 can be realized. This corresponds to elongations of the chemical bonds on the order of 10–20%, leading to dissociation. In brittle materials such as fused quartz or crystalline silicon, bond dissociation leads to failure and the formation of cracks.

Experimental

In the present experiments fused quartz samples (Herasil I) and silicon single crystals with (111), (110), and (100) surface orientation were investigated. The surfaces of the silicon and fused quartz samples were polished to high optical quality and normally used as received.

Nonlinear SAW pulses were excited using Nd:YAG laser radiation (wavelength 1.06 µm, duration 8 ns, pulse energy up to 150 mJ). The laser beam was focused into a strip of length ~8 mm and width ~10 µm. In the region of the excitation line the sample surface was covered with a thin strongly absorbing carbon layer in the form of an aqueous suspension. Irradiation of such a suspension with short laser pulses leads to overheating and explosive evaporation of this liquid film. This results in a strong transient normal force acting on the surface, which generates nonlinear SAW pulses with high amplitudes.

The transient SAW pulses were detected with a probe beam deflection setup using a stabilized diode-pumped continuous wave (cw) Nd:YAG laser (wavelength 532 nm, power up to 100 mW). The cw laser beam was divided into two parts of approximately the same intensity. Each probe beam was sharply focused by a gradient-index lens into a spot of approximately 4 µm diameter on the sample surface, forming two probe spots along the SAW path. The deflection of the probe beam due to the transient SAW pulse was monitored with a position-sensitive detector. Since the deflection effect depends on the slope of the surface distortion, the velocity normal to the surface, the so-called velocity profile or shear component $u_{3,1}$ is measured [1]. The bandwidth of the entire detection setup was limited by the finite probe size to about 500 MHz. The deflection signal, which is proportional to the surface slope of the

transient SAW pulse, was amplified and recorded by an oscilloscope with 1 GHz bandwidth.

Nonlinear SAW profiles

Contrary to nonlinear elastic distortions in fluids, those in SAWs may result in an increase of stress with propagation distance. However, this growth of stress is limited by frequency-dependent damping processes, which we assume to be proportional to the frequency squared. If the characteristic shock formation length is sufficiently small in comparison to the attenuation length of the material, the stress accumulated after a certain propagation distance can reach the mechanical strength, causing failure of the solid.

In isotropic fused quartz the nonlinear distortions in the propagating SAW pulse result in the formation of a U-shaped surface velocity profile with spikes. The experimentally measured pulse shapes are shown in Fig. 1 in comparison with the theoretical simulation based on the evolution equation described in [4]. At the remote probe location the comparison indicates a substantially extended frequency range, which obviously cannot be resolved experimentally due to the finite size of the probe spot. Therefore the predicted waveform has larger spikes than the experimental one. The reasonable agreement between experiment and the theoretical prediction seems to confirm the correctness of the theoretical model and the procedure applied to calibrate the waveforms.

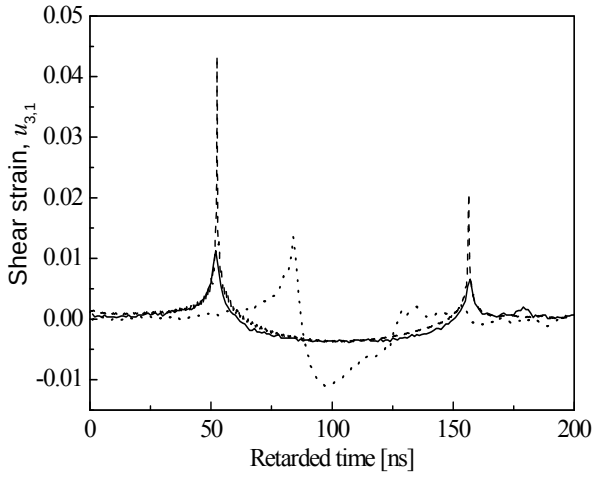

Fig. 1 Shear strain component $u_{3,1}$ of nonlinear SAW profiles in fused quartz at distances 1 mm (dotted line) and 16 mm (solid line) from the source. The simulated waveform is shown as a dashed line.

As mentioned before, the nonlinear behavior of different silicon planes and directions were investigated. The Si(111) plane and the <112> directions were selected for fracture experiments because of the high value of the coefficient of nonlinearity and the suppression of diffraction in this geometry. Moreover, the evolution of the SAW pulse can be accurately calculated, since the second- and third-order elastic constants are well known for silicon. Figure 2 shows the development of the surface velocity profiles measured for SAW propagation in the [11-2] and the [-1-12] directions on Si(111) at the two probe spots. The surprising effect of very different pulse shapes generated in the two opposing directions is explained by the symmetry properties of the selected Si(111) plane and directions in the anisotropic silicon crystal, without referring to an eventual fracture process [5].

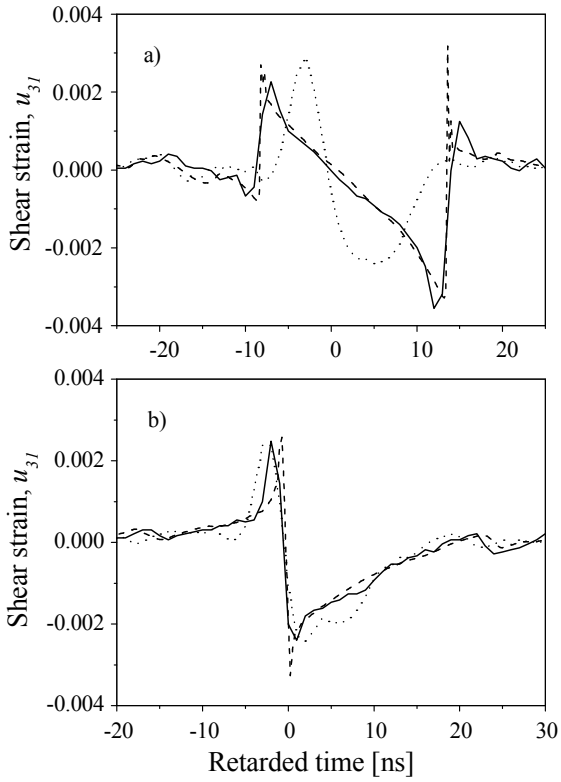

Fig. 2 Evolution of nonlinear SAWs on Si(111) for pulses propagating in a) the [11-2] direction and b) the [-1-12] direction. Dotted lines: waveforms measured at 3 mm; solid line: waveform measured at 18 mm; dashed lines: calculated waveform.

The nonlinear evolution of the SAW pulse can be interpreted as an interaction between different spectral components of the surface inclination governed by nonlinear matrix elements, which depend on the second-order and third-order elastic constants. Thus, pulse evolution can be calculated by a system of coupled evolution equations. The corresponding matrix describes both the local nonlinearity (existing also in fluids) and nonlocal nonlinearity, which appears only in Rayleigh waves. Real values of the matrix elements lead to the development of N-type distortions, as

observed in the Si(111) case, and imaginary values generating U-shaped waveforms as found in fused quartz.

Solitary SAW pulses

While solitary waves on a water surface, which are connected with gravitational forces, were observed as early as 1834 by John Scott Russel and have been thoroughly studied experimentally, there was no clear experimental observation of their elastic counterparts at the surface of a solid for a long time. Recently solitary SAW pulses were observed in a laser-based pump-probe experiment by compensating the two major sources of SAW pulse deformation [6]. The nonlinearity was matched by dispersion generated by loading or stiffening the surface with a thin layer.

In order to identify a single solitary pulse, it is favorable to start with a short high-intensity acoustic pulse. To realize a solitary surface wave, the elastic nonlinearity of the solid has to be balanced by dispersion. Nondispersive Rayleigh waves become dispersive when the elastic medium is covered by a film with different properties that introduces a length scale and gives rise to an acoustic mismatch at the interface. By selecting suitable coatings, both normal and anomalous dispersion were matched with the nonlinearity of the excited SAW pulses. This strategy made it possible to generate and detect two different types of solitary surface waves [6].

The solitary regime of SAW propagation requires a sufficient level of elastic deformations in the wave profile. Therefore the nonlinear distortion length must be smaller than the propagation distance. In this case the effects of nonlinearity are accumulated in the traveling SAW pulse. A drastic increase of the SAW magnitude, however, can lead to sample fracture due to shock front formation. Within the present propagation lengths of typically 2 cm, suitable nonlinear distortions were observed for an acoustic Mach number of the order of $M \approx 3\times10^{-3}$, whereas for $M \approx 10^{-2}$ the fracture strength of most materials is reached.

In isotropic fused silica normal dispersion was obtained by deposition of a film consisting of a NiCr alloy (80% Ni, 20% Cr). The film thickness of about 300 nm, needed to obtain a single solitary pulse at the remote probe location, was estimated by means of numerical simulations.

The solitary pulse monitored at the remote probe location 17 mm away from the source is depicted in Fig. 3 as a solid line. At the first probe spot a compact pulse with about 20 ns duration was registered. The evolution resulted in the generation of a short bipolar pulse traveling at a speed higher than the linear Rayleigh velocity and in a weak oscillatory tail moving with lower velocity. This so-called radiation resembles the behavior of a Korteweg–de Vries (KdV) soliton. Note that its amplitude is not sufficient for the generation of a significant nonlinear effect. Thus the mean propagation velocity of this part is lower than the Rayleigh velocity.

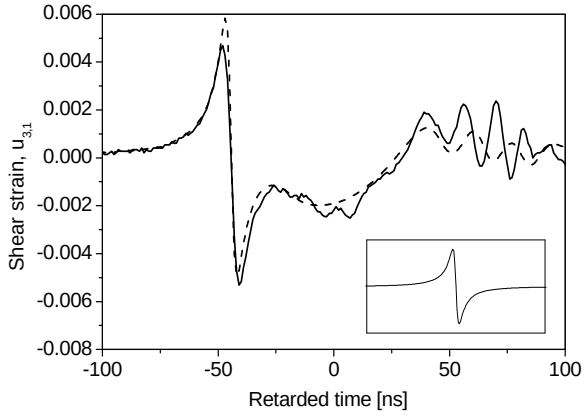

Fig. 3 Evolution of solitary pulse shapes for normal dispersion (fused silica with NiCr layer). Dashed line: simulation using the evolution equation; inset: theoretical stationary solution.

The dispersive nonlinear evolution equations developed for a theoretical description of the experimentally observed pulse shapes deviate from the KdV equation [7]. This fact stresses the special features of solitary surface waves in comparison to solitary water waves and bulk solitons. The theoretical stationary profile calculated numerically for this particular system is shown in the inset of Fig. 3. The spatial evolution of the SAW pulse in fact leads to the formation of a pulse with the predicted stationary shape.

In the numerical simulations of solitary pulses based on the evolution equation the signal from the first spot was substituted into the evolution equation as an initial condition. The initial problem for this equation was solved numerically and the result of the evolution at the remote probe location is shown in Fig. 3 as a dashed line. Since this model describes the pulse evolution in very good agreement with the experiments it is possible to simulate the shape of the solitary pulse also for larger propagation distances and to reconstruct the development of the pulse between the two probe spots. The result is shown in Fig. 4 in a two-dimensional form. Here the propagation distance is plotted versus the retarded time. Note that the distance is given with respect to the first probe spot; hence zero corresponds to the profile measured at the first probe spot. Thus the signal depicted in Fig. 3 corresponds in Fig. 4 to a distance of 15 mm. As is evident, the bipolar pulse essentially conserves its shape. This becomes apparent in a comparison with the behavior of the oscillatory tail, which significantly broadens with

propagation due to the dispersion effect, despite its much narrower bandwidth.

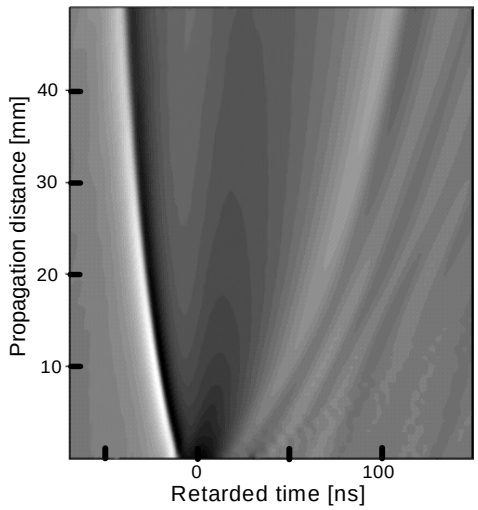

Fig. 4 Simulation of solitary SAW pulse evolution with distance from the first probe spot.

The width and velocity of the solitary pulse depend on its amplitude. At the beginning it propagates faster, but as the amplitude decreases due to dissipation, the velocity decreases, approaching the linear Rayleigh velocity, whereas the pulse width increases. These features are similar to the Benjamin–Ono (BO) solitons. The longitudinal velocity component of the signal $u_{1,1}$ is related to the measured $u_{3,1}$ component by the Hibert transform. The bipolar solitary pulse in the shear component $u_{3,1}$ corresponds to a typical "Mexican hat" shape in $u_{1,1}$.

To change the sign of the dispersion effect we deposited a "stiffening" film onto fused silica. As the coating we selected titanium nitride, which possesses a high stiffness. The numerical estimations for the optimal film thickness provided a value of about 50 nm. The profile measured at the remote location behaves mirror symmetric to the case of normal dispersion: the bipolar solitary pulse has an opposite polarity and a velocity lower than the linear Rayleigh velocity in uncoated fused silica samples. Numerical simulations carried out in the same way as for normal dispersion show a satisfactory agreement with the experiment.

The character of nonlinear SAW evolution in crystals can differ substantially from that in isotropic media. For example, pulse evolution on the Si(111) cut in the [11-2] direction transforms the short initial pulse into a broadened N-shaped profile (see Fig. 2a). For the wave propagating in the opposite [-1-12] direction the evolution becomes mirror symmetric with respect to retarded time. For both directions the theoretically predicted stationary solutions have slightly asymmetric "Mexican hat" shapes in $u_{3,1}$, but their polarities are opposite. This asymmetry reflects the fact that in this case the free surface is not parallel to the plane of mirror symmetry of the crystal.

To realize normal dispersion the Si(111) surface was oxidized thermally at 900°C. The thickness of the silicon-dioxide layer was about 110 nm. Solitary pulses with the predicted "Mexican hat" shapes were observed in the [-1-12] direction only, as shown in Fig. 5. The solid line designates the experimentally registered pulse, the dashed line shows the simulation with the evolution equation. The inset presents the theoretical stationary solution for this particular system. Note that the "Mexican hat" is formed in the $u_{3,1}$ profile, unlike the cases of an isotropic substrate or highly symmetric crystal surfaces, such as the Si(001) plane, where the $u_{1,1}$ component has a stationary solution with such a shape.

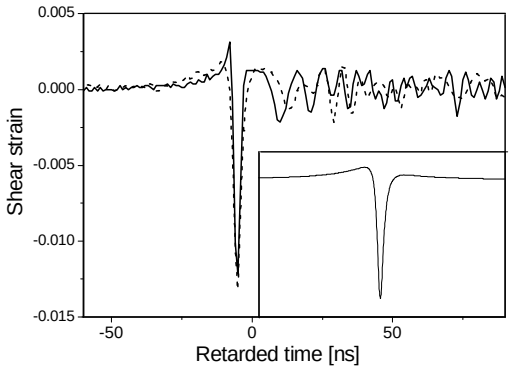

Fig. 5 Evolution of solitary pulse shapes for normal dispersion in the system Si(111) with a SiO_2 layer.

The measured and computed solitary pulse shapes are strongly influenced by the anisotropy of the substrate. In separate numerical simulations pulse collisions were investigated for different dispersion laws that result from the specific acoustic mismatch between film and substrate. For a special type of linear dispersion the occurrence of almost elastic pulse collisions was demonstrated [7].

Stress in SAW pulses

In isotropic media there is no a priori preferred orientation for crack nucleation and growth at high Mach numbers. In order to determine the optimal conditions for fracture by strongly nonlinear SAW pulses, the angular dependence of the peak longitudinal "opening" stress was calculated for the experimentally measured waveforms. The measured velocity profiles $u_{3,1}$, such as those shown in Fig. 1, determine uniquely the wave field at every instance and at any depth in the sample. For the evaluation of this field we used the exact solution of the conventional linear surface wave

problem. This provides the complete set of eigenvalues: the phase velocity, the depth distribution, and the polarization vectors for all partial waves. The $u_{3,1}$ profile is extended into a Fourier series, and the wave field $u_{i,j}(x_1,x_3)$, where x_1 is the propagation direction and x_3 the direction normal to the surface, is calculated as a superposition of the wave fields of all spectral components. The next step is to calculate the stress tensor field: $\sigma_{ij} = C_{ijkl}u_{k,l}$, where C_{ijkl} designates the second-order elastic stiffness tensor. Finally we transform the stress tensor to the new coordinate system tilted into the specimen by an angle φ. In this new coordinate system the stress component σ_{11} represents the "opening" stress, directed normal to the conjectured cracking plane. Applying the linear elasticity approximation here assumes the smallness of all the values $u_{i,j}$. This condition holds well in the SAW pulses considered, since the displacement gradients are naturally limited to the order of 10^{-2} due to materials failure.

The results obtained indicate that for fused quartz the stress attains its maximum value in the direction of wave propagation with $\varphi = 0$. Thus the crack is expected to grow perpendicularly to the surface if the opening mode (mode I) cracking behavior prevails. In corroboration with the traction-free boundary condition at the surface, the stress vanishes for φ = 90°. The spatial-temporal distribution of σ_{11} ($\varphi = 0$) for the experimental SAW pulse shown in Fig. 1 by the solid line is presented in Fig. 6. The stress distribution has a sharp peak at the surface, therefore the onset of fracture is expected to occur in the vicinity of the surface.

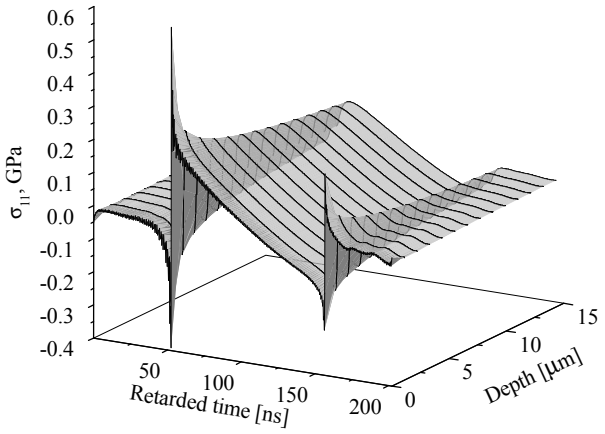

Fig. 6 Calculated spatial-temporal distribution of the opening stress σ_{11} at $\varphi = 0$ for the SAW pulse shown in Fig. 1.

In anisotropic materials, such as silicon, the character of the stress field generated in a nonlinear wave varies substantially with the plane orientation and the wave propagation direction. The same procedure as described above can be applied to calculate the spatial-temporal distribution of the opening stress σ_{11}, directed normal to the cleavage plane for the two pulses presented in Fig. 2. Here, we consider again the propagation of a finite-amplitude SAW pulse along the Si(111) surface in the <112> directions. Note that the crystal is not mirror symmetric with respect to the (112) plane. This results in opposite signs of the shock fronts generated and different stress distributions observed in the evolutions of nonlinear SAW pulses propagating along the [11-2] and [-1-12] directions. As discussed later on, this is the reason for the characteristic differences in the fracture behavior.

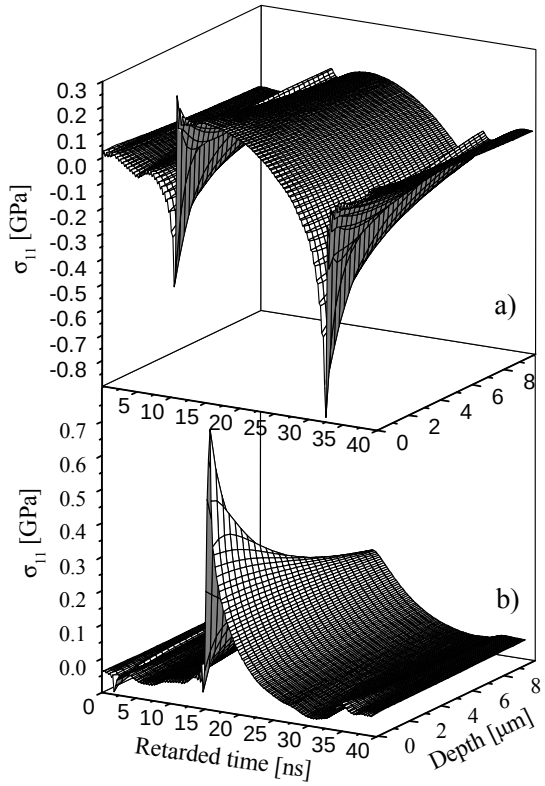

Fig. 7 Calculated spatial-temporal distribution of the σ_{11} component perpendicular to the cleavage plane for the pulse propagating in a) the [11-2] direction and b) the [-1-12] direction.

Fracture of fused quartz

Fracture of fused quartz (Herasil I) was studied as an example of a nonlinear isotropic material. Of special interest is the strain distribution at the area located close to the first probe location because cracks were observed in this case. Obviously the nonlinearity of the SAW pulse developed at this point was sufficient to fracture the brittle samples. Note that the peak intensity of the real waveform may be much higher than

measured due to the experimental bandwidth limitations.

Since the isotropic amorphous material has no preferred cleavage planes, unlike silicon, the nucleation of cracks is expected to occur perpendicular to the direction of highest tensile stress or strain in the case of mode I cracking. A whole field of cracks was clearly visible at the surface (see Fig. 8) and appeared at a distance of several hundred micrometers to a few millimeters from the laser excitation line. After nucleation, expected to occur originally perpendicular to the SAW propagation direction at the sample surface, the cracks bend forward, symmetrically on both sides, in the direction of SAW propagation, extending into different angles and branches.

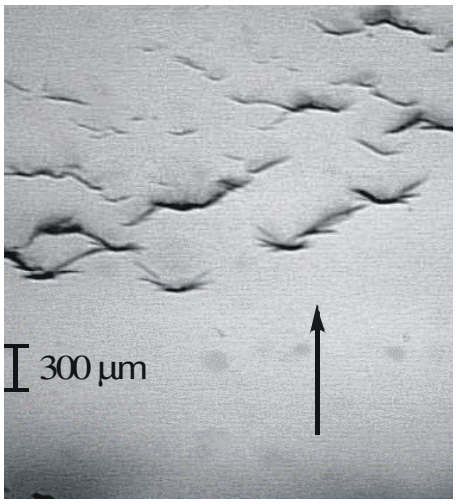

Fig. 8 Optical microscope picture of the crack features at about 1-2 mm from the SAW excitation line in fused quartz. The arrow indicates the SAW propagation direction.

The propagation of the cracks into the bulk material was investigated by probing different depths with the focus of a confocal laser microscope. The intensity of the backscattered light was used to track the orientation of a particular crack into the bulk. Within the inherently large error involved for determining the angle of penetration into the depth, the measurements indicate that the cracks penetrate at ~30–35° to the surface in the direction of SAW propagation.

These results are consistent with the scenario that the cracks nucleate at the surface, where the particle displacements and the longitudinal opening stress in the SAW pulse reach their maxima. According to the calculated opening stress the nucleated microcracks may expand first short distances perpendicular to the direction of wave propagation along the surface and into the bulk. Then, under the influence of the displacements field of the SAW pulse, the expanding cracks turn partially towards the direction of SAW propagation, forming characteristic forward-bending surface patterns. After several micrometers of normal growth into the depth, further penetration into the solid occurs at an angle of ~30-35° to the SAW propagation direction. Since the displacement field decays strongly with depth it is expected that crack extension should be longer along the surface than into the bulk but penetration into the solid could not be estimated.

The partial change of crack propagation into the direction of SAW propagation at the surface and in the depth seems to be a characteristic feature of isotropic fused quartz. This behavior can be understood, at least qualitatively, by the tendency of the crack to move with the opening stress provided by the propagating SAW pulse. Thus fracture proceeds under the influence of the transient stress field after the nucleation process.

Fracture of silicon

In the calculated spatial-temporal stress component normal to the {11-1} cleavage plane of the two SAW pulses presented in Fig. 2, positive stress denotes stretching of the material, whereas a negative one is associated with compression. Accordingly, the N-type pulse moving in the [11-2] direction exhibits two short compression peaks, while the [-1-12] pulse has one strong tensile peak. Thus the SAW pulse formed in the [-1-12] direction is expected to induce fracture more easily along the weakest silicon cleavage plane than the one running in the opposite direction, if mode I fracture dominates [5].

Indeed, the SAW experiments reveal a significant difference in the laser pulse energies needed to induce fracture without seed crack. In the [11-2] propagation direction cracks were observed only for laser pulse energies exceeding 120 mJ, whereas in the opposite direction the threshold was as low as 30 mJ. Therefore, under suitable conditions cracks appeared only on one side of the source, namely in the [-1-12] direction, and the wave propagating in the [11-2] direction could be used to determine the corresponding SAW amplitude. This was realized by gradually increasing the laser pulse energy until fracture was observed at one side of the source. In this way, the SAW amplitude at the cracking threshold was evaluated, yielding the critical tensile stress for the weakest cleavage plane of silicon. From the spatial-temporal distribution of the stress at the cracking threshold, a critical tensile stress of about 1.6 GPa was extracted for dynamic fracture of the silicon sample employed [5].

The SAW-induced cracks were detected at the sample surface by scanning force microscopy (SFM), as shown in Fig. 9. A strongly nonlinear SAW pulse creates a whole field of cracks extending essentially along the <110> direction, perpendicular to the <112> direction of SAW propagation. The characteristic topographical saw-tooth-like surface displacements observed are in

the range of 10-30 nm with a separation of the individual cracks of the field of 15-30 µm.

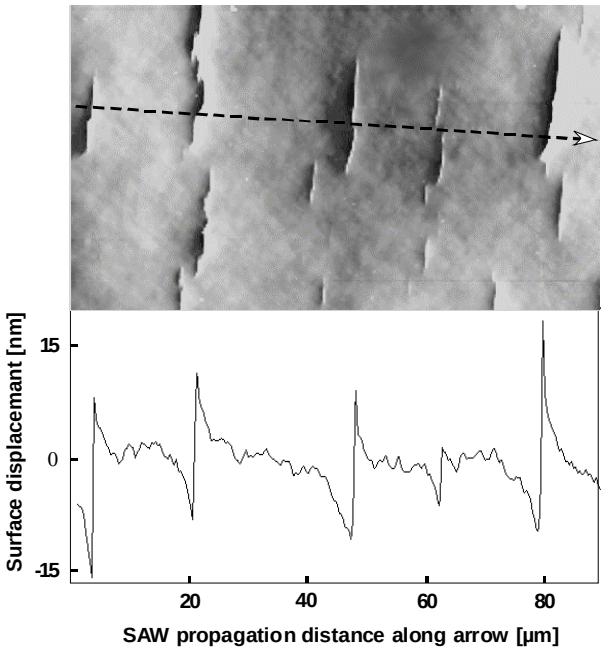

Fig. 9 a) SFM image of the fractured Si(111) surface. The arrow in a) indicates the direction of SAW propagation. b) Topographical cross section of the surface along the arrow.

In Fig. 10 a focused ion beam (FIB) image of crack extension into the bulk of silicon is presented. The SAW pulse propagated from left to right in the easy cracking [-1-12] direction, generating strong tensile loading. For this FIB measurement an individual crack located at a distance of about 800 µm from the source was selected. The interior surface shown, which was opened by the FIB cut, is always normal to the sample surface. The crack presented extends into the sample at an angle of ~71° to the direction of the incoming SAW pulse at the surface. Within the accuracy of these measurements this is the angle between the Si(111) surface plane and the {11-1} cleavage plane. Around a depth of 3.5–4 µm the crack suddenly changes direction. Beyond a depth of about 4 µm it continues perpendicular to the surface into the solid. This corresponds approximately to a {112} cracking plane. Further extension of this crack into the bulk could not be resolved because it was not possible to cut deeper into the solid with the FIB technique. It is interesting to note that the crack tip propagated backwards with respect to the direction of the traveling SAW pulse in the easy cracking case.

In addition, bulk penetration of a crack that was initiated by a SAW pulse propagating along the Si(111) plane in the opposite direction, namely [11-2], was studied, where compressional loading dominates.

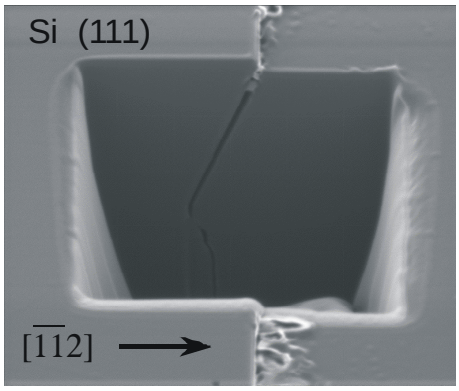

Fig. 10 FIB image of crack penetration into the bulk from the Si(111) surface. The SAW pulse propagated from the left to the right in the [-1-12] direction. In the picture the angle between the sample surface and image plane is 45°.

From the surface the crack first extends into the solid along the {11-1} cleavage plane up to a depth of about 4 µm, where it changes direction irregularly until again the {112} plane is reached at a depth of about 6–10 µm. Interestingly, near the surface the cleavage plane extends here into the bulk in the direction of SAW propagation.

The detailed results obtained for different crystal planes and directions suggest the following conclusions for impulsive SAW fracture of single-crystal silicon. Even under the impulsive loading conditions employed crack nucleation occurred on Si{111} cleavage planes, while crack propagation can make use of {110} and higher index planes. The analysis of the stress field indicates that the higher tensile stress found for the [-1 -12] propagation direction dominates fracture, even if the corresponding {11-1} cleavage plane is backward oriented. This dominance of the {111} cleavage planes over other planes is consistent with the theoretical fracture strength of the main silicon planes estimated on the basis of Griffith's theory. By inserting the distance between the atomic planes parallel to the particular crack plane into the relevant expression a variation of the mechanical strength according to {111} < {110} < {100} is found [9].

The stresses at which cracks were nucleated on the weakest Si{11-1} cleavage plane intersecting the Si(111) surface were estimated to be of the order of 1–2 GPa. This is substantially lower than the theoretical fracture strength of the Si{111} cleavage plane of about 33 GPa. A comparable value is obtained with the very simple bond-extension model, which assumes that bond dissociation takes place at a bond extension of 10–20%. With a mean Young's modulus of 160 GPa and $\Delta l/l$ = 0.15 the corresponding critical stress is about 24 GPa. The large discrepancy between the experimental result

and theory seems to exclude homogeneous crack nucleation. Accordingly, in the spirit of Griffith's theory the much lower experimental value suggests the existence of submicrometer cracks with a size on the order of roughly 100 nm as the origin of growing cracks. Thus dynamic fracture is expected to start at already existing intrinsic submicrometer defects or flaws located at or near the surface and follows the weakest cleavage planes.

An important property of SAWs is their elliptical polarization with longitudinal and shear displacement components. The theoretical analysis of the various effects is very complicated and still at the beginning. Besides mode I tensile loading considered here, also mode II contributions from the shear components may come into play. The effect of mode II in-plane sliding can be clearly seen in the SFM topography (see Fig. 9), where the two cracking planes exhibit a relative shift of about 10–30 nm against each other. The effect can also clearly be seen in Fig. 10.

Conclusions

Strongly nonlinear surface waves, launched by the absorption-layer method and investigated with the laser-based pump-probe setup, provide a new tool in materials science [8]. By matching nonlinearity with geometrical dispersion, introduced with a thin loading or stiffening film, solitary SAW pulses were observed. Nonlinear evolution of the pulse shapes is observed during propagation if the attenuation length is smaller than the shock formation distance. Another important feature of surface waves is that the energy remains localized at the surface within the depth of about one wavelength. Hence the generation of higher harmonics leads to an increase of the energy density within the correspondingly smaller penetration depth. For these reasons, Mach numbers or strains in the range of 10^{-3}–10^{-2} can be realized, where materials normally fail. This fact opens a new door to dynamic fracture mechanics. It can be anticipated that due to the achievable strong nonlinearity of broadband nonlinear SAW pulses they are expected to make important contributions to the field of dynamic fracture in the near future.

Acknowledgments

The authors thank the Deutsche Forschungsgemeinschaft (DFG) for financial support and AML for a fellowship.

References

[1] A. Lomonosov, A. P. Mayer, and P. Hess, in *Modern Acoustical Techniques for the Measurement of Mechanical Properties*, edited by M. Levy, H. E. Bass, and R. Stern, Vol. 39**,** pp. 65-134, Academic Press, Boston, 2001.

[2] Al. A. Kolomenskii, A. M. Lomonosov, R. Kuschnereit, and P. Hess, "Laser generation and detection of strongly nonlinear elastic surface pulses", Phys. Rev. Lett. 79, pp. 1325-1328, 1997.

[3] A. Lomonosov and P. Hess, "Effects of nonlinear elastic surface pulses in anisotropic silicon crystals", Phys. Rev. Lett. 83, pp. 3876-3879, 1999.

[4] G. Lehmann, A. M. Lomonosov, P. Hess, and P. Gumbsch, "Impulsive fracture of fused quartz and silicon crystals by nonlinear surface acoustic waves", J. Appl. Phys. 94, pp. 2907-2914, 2003.

[5] A. M. Lomonosov and P. Hess, "Impulsive fracture of silicon by elastic surface pulses with shocks", Phys. Rev. Lett. 89, pp. 095501-1-4, 2002.

[6] A. M. Lomonosov, P. Hess, and A. P. Mayer, "Observation of solitary elastic surface pulses", Phys. Rev. Lett. 88, pp. 076104-1-4, 2002.

[7] A. P. Mayer, A. M. Lomonosov, P. Hess, C. Eckl, and A. S. Kovalev, "Solitary surface acoustic waves", in: *Nonlinear Acoustics at the Beginning of the 21st Century*, edited by O. V. Rudenko and O. A. Sapozhnikov, Faculty of Physics, MSU, Moscow, Vol. 1, pp. 65-68, 2002.

[8] P. Hess, "Surface acoustic waves in materials science", Physics Today, 55, pp. 42-47, 2002.

[9] F. Ericson and J-Å. Schweitz, "Mechanical properties of materials in microstructure technology", in: *Handbook of Micro/Nano Tribology*, edited by B. Bhushan, CRC Press, Boca Raton, pp.763-796, 1999.